nature catalysis

Article

https://doi.org/10.1038/s41929-023-01094-0

An electrochemical approach for designing thermochemical bimetallic nitrate hydrogenation catalysts

Received: 29 March 2023

Accepted: 1 December 2023

Published online: 19 January 2024

Check for updates

Kunal M. Lodaya[1,3], Bryan Y. Tang[1,3], Ryan P. Bisbey[1], Sophia Weng[1], Karl S. Westendorff[2], Wei Lun Toh[1], Jaeyune Ryu[1], Yuriy Román-Leshkov[1,2] & Yogesh Surendranath[1,2]

Classically, catalytic promotion in bimetallic catalysts has been ascribed to atomic-scale cooperativity between metal constituents. For catalytic reactions that could involve charge transfer, electron and ion flow may engender bimetallic promotion without atomic-level connectivity. Here we examine this hypothesis in the context of nitrate hydrogenation, a reaction catalysed almost exclusively by bimetallic catalysts. On state-of-the-art PdCu/C, nitrate hydrogenation to nitrite proceeds via electrochemical coupling of hydrogen oxidation and nitrate reduction half-reactions; Pd catalyses the former, while Cu catalyses the latter. Using this mechanistic framework, we predict how different Pd:Cu ratios affect nitrate hydrogenation rates, and rationalize the catalytic activity observed in PtAg/C and Ru/C. Finally, by only promoting the electrochemical hydrogen oxidation reaction with $Ni(OH)_2$, we synthesize $PdNi(OH)_2Cu/C$ catalysts with comparable nitrate hydrogenation activity to our best-performing PdCu/C using fivefold less Pd. This work provides an alternative strategy for designing alloy catalysts for thermochemical redox transformations.

Bimetallic catalysts have an enormous range of reactivity spanning aerobic oxidations, selective hydrogenations of hydrocarbons, small-molecule electrochemical transformations and cross-coupling reactions[1–5]. Uncovering the origin of enhanced activity and/or selectivity when compared with monometallic counterparts is essential to the rational design of improved catalysts. Classically, the unique reactivity of bimetallic catalysts has been attributed to either ligand/strain effects or ensemble effects[6–10]. Ligand/strain effects arise from electronic structure perturbations of one metal by the other that tune adsorption strengths of intermediates and thereby modulate reactivity[11]. In contrast, ensemble effects refer to the population and distribution of metal atoms proximate to the active site. These effects can alter the adsorption modes of intermediates, introduce spillover of intermediates from one site to another and encompass catalyst–support interactions[12]. Importantly, most of these classical modes of action in bimetallic catalysis require intimate, atomic-level contact between the alloy components or between metal components and support, with spillover effects potentially occurring over longer length scales with conductive supports[13].

As a poignant example, the above paradigms have been used to rationalize the reactivity of bimetallic catalysts for nitrate hydrogenation. This reaction, which is of importance in the context of waste-water remediation, has been found to require bimetallic catalysts to proceed at measurable rates[14]. While nitrate can be hydrogenated to a wide diversity of products including NO, NO_2, N_2 and ammonia, the initial hydrogenation from nitrate to nitrite is viewed to be rate limiting[15,16]. For this reaction step in particular, monometallic catalysts all show greatly reduced or no activity. The two metals paired for thermochemical nitrate hydrogenation are typically a noble metal such as Pd or Pt alongside a promoter metal, such as Cu, In or Sn, with PdCu

[1]Department of Chemistry, Massachusetts Institute of Technology, Cambridge, MA, USA. [2]Department of Chemical Engineering, Massachusetts Institute of Technology, Cambridge, MA, USA. [3]These authors contributed equally: Kunal M. Lodaya, Bryan Y. Tang. e-mail: yogi@mit.edu

https://doi.org/10.1038/s41929-023-01094-0

being the most well-studied and best-performing pairing[17–24]. Various proposals have been offered to explain the enhanced activity compared with monometallic systems and the respective role of each metal. The prevailing hypotheses include hydrogen spillover from Pd sites to Cu sites, or Langmuir–Hinshelwood bimolecular recombination at mixed PdCu active sites[16,25,26]. Both mechanisms align with the classical picture of bimetallic catalysis, requiring atomic-level contact between the two metals.

In recent years, there has been a growing appreciation that liquid-phase thermochemical catalysis can proceed via the electrochemical coupling of countervailing half-reactions mediated by the exchange of band electrons[27–30]. This band-mediated mechanism for liquid-phase thermochemical catalysis was shown to be operative across a range of aerobic oxidations in monometallic catalyst systems[31] and has been applied in the context of H_2O_2 synthesis on a variety of Pt- and Pd-based catalysts[32,33]. This mechanism has also been shown to be operative for aerobic hydroquinone oxidation at molecular active sites embedded within metallic solids[34]. Electrochemical coupling is also possible across disparate active sites capable of performing distinct reactivity, such as in the coupling of Pd/C with enzyme redox catalysis[35]. Recently, a band-mediated catalytic mechanism was also suggested for an alloy system conducting aerobic oxidation at AuPd catalyst active sites[36]. In that work, simple mixtures of Au/C and Pd/C display activity enhancements for alcohol oxidation, though the electrochemical mechanism underpinning this reactivity remains ill defined. Given that many of the constituent metals employed for thermochemical nitrate hydrogenation also display activity for electrochemical nitrate reduction[37–41], we postulated that band-mediated mechanisms may be operative for this reaction class as well, and that electrochemical analysis of this reaction could shed light on the origin of bimetallic promotion.

Despite the growing appreciation of the role of electrochemical pathways in thermochemical catalysis, to the best of our knowledge, there remains little insight into how electrochemical reactions partition across bimetallic catalysts. For example, in one limiting extreme, each individual component of the bimetallic system is capable of carrying out both half-reactions. In this limit, despite an electrochemical coupling mechanism, the aggregate activity of the alloy is expected to be the sum of the activities of each individual component. However, in the other limiting extreme, wherein each alloy component is only able to carry out one of the half-reactions, electrical contact, but not atomic-level contact, between alloy components is the sole prerequisite for carrying out the overall reaction. Consequently, distinguishing between these two limiting cases has important implications for the design of high-performance alloy catalysts.

In this Article, we show that nitrate hydrogenation to nitrite on PdCu/C proceeds via the latter extreme. Using electrochemical tools, we show that Pd carries out electrochemical hydrogen oxidation to protons and electrons and has no activity for nitrate reduction. In contrast, we find that Cu is active for nitrate reduction with no activity for hydrogen oxidation. This complete separation in the functional role of each alloy component provides a pathway for the design of bimetallic catalysts for the net thermochemical reaction by pairing pure metals with electrocatalytic activity for each complementary half-reaction. Employing this strategy, we identify promising materials for nitrate hydrogenation catalysis with equal or improved performance relative to state-of-the-art PdCu/C. These results highlight how electrochemical analysis of thermal reactions provides opportunities for catalyst discovery.

Results

PdCu/C performs hydrogen oxidation and nitrate reduction

To examine whether a band-mediated electrocatalytic mechanism is operative for thermochemical nitrate hydrogenation to nitrite, we deployed a similar experimental framework to that used in our previous studies of aerobic oxidation catalysts, originally developed and deployed broadly in the field of corrosion science[31,34,42,43]. Briefly, we collect voltammetric data for the putative electrochemical half-reactions that comprise the net thermochemical transformation. By applying a current matching condition to the electrochemical data for each half-reaction in isolation, we extract a predicted open circuit potential (OCP) and reaction rate for the net thermochemical reaction. Comparing these values with those measured under hydrogenation conditions provides a quantitative measure of whether a band-mediated electrocatalytic mechanism is operative.

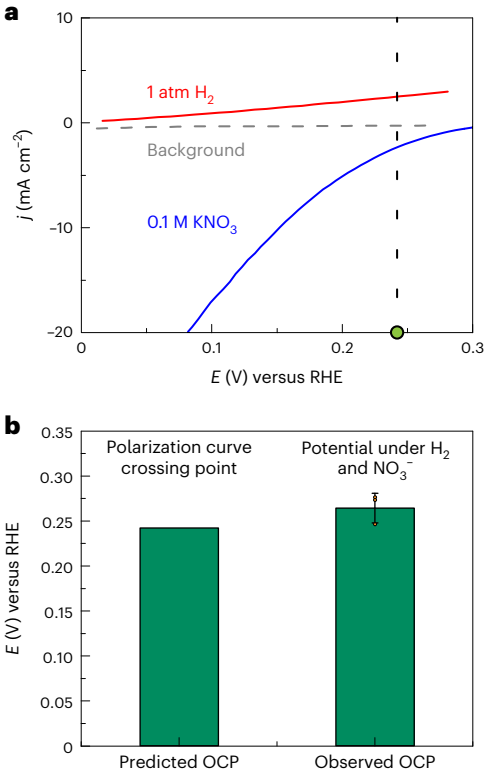

Fig. 1 | Electrochemical polarization data for PdCu/C predicts OCP during catalysis. a, Polarization curves recorded via LSV at 2 mV s^{-1} scan rate of a PdCu/C (10:90 molar ratio) GDE in 0.2 M KOH. Background trace (dashed grey) was collected under 1 atm Ar; 0.1 M KNO_3 trace (blue) was collected under 1 atm Ar; 1 atm H_2 trace (red) was collected in the absence of KNO_3. Black dashed line indicates the potential at which the currents for the blue and red traces are equal and opposite, with an x intercept of 0.24 V versus the reversible hydrogen electrode potential (RHE). All current densities are normalized with respect to the geometric surface area of the electrode. **b**, OCP value under thermochemical reaction conditions (1 atm H_2 + 0.1 M KNO_3), predicted from the polarization curves (left), and measured (right). Error bar represents standard deviation of three replicate experiments, with the centre being the mean and dots representing potential measurements from each replicate experiment.

Electrochemical measurements and thermochemical reaction data were collected under two electrolyte and pH conditions. For the majority of experiments, 0.1 M KNO_3 + 0.2 M KOH (pH 13) was used to enable faster reaction rates as well as a simplified product distribution. Experiments yielding key findings were then expanded to 0.1 M KNO_3 + 0.5 M phosphate buffer (pH 6.7) to more closely approximate typical experimental conditions probed in the literature[17]. To draw direct comparisons between electrochemical and thermochemical measurements, we fabricated electrodes suitable for both modes of study. Critically, these electrodes required both high catalyst loading and efficient gas transport of H_2 to achieve high thermochemical reaction rates of hydrogenation with minimal effects from H_2 transport limitations. Thus, we employed gas-diffusion electrodes (GDEs) with dropcast catalysts for all measurements (catalyst synthesis,

https://doi.org/10.1038/s41929-023-01094-0

characterization, electrode fabrication and experimental details in Methods as well as Supplementary Methods and Supplementary Figs. 7–15). PdCu/C at a 10:90 molar ratio of Pd:Cu was chosen to begin this investigation because of the extensive body of research on nitrate hydrogenation with this particularly alloy[17,20,21].

We began by measuring steady-state polarization behaviour via linear-sweep voltammetry (LSV) at 2 mV s^{-1} on a PdCu/C GDE. These measurements were performed under two conditions: 1 atm H_2 with no KNO_3, and 0.1 M KNO_3 under 1 atm Ar. In the presence of H_2 and the absence of nitrate, we observe the onset of anodic current beginning at 0 V versus the reversible hydrogen electrode potential (RHE), rising to 5 mA cm^{-2} at ca. 0.3 V (Fig. 1a, red). In contrast, in the presence of nitrate and absence of H_2, we observe the onset of cathodic current of 0.4 mA cm^{-2} at ca. 0.3 V, with 20 mA cm^{-2} observed at ca. 0.1 V (Fig. 1a, blue). These data suggest that PdCu/C is capable of catalysing two distinct half-reactions depending on the reaction conditions: the hydrogen oxidation reaction (HOR) and the nitrate reduction reaction (NO_3RR). Importantly, the potential range for NO_3RR matches that of HOR, with equal and opposite currents at ca. 0.24 V versus RHE (Fig. 1a, vertical dotted line). Subjecting the same PdCu/C GDE to thermochemical catalysis conditions—with both NO_3^- and H_2 present—we observe that the OCP of the catalyst (which is the electrode potential in the absence of external polarization) rapidly reaches a steady-state value of 0.26 V versus RHE (Fig. 1b). The same analysis was conducted with different formulations of PdCu at 50:50 and 90:10 ratio, with the former yielding a predicted OCP of 0.19 V and observed OCP of 0.17 V, and the latter yielding a predicted OCP of 0.14 V and observed OCP of 0.11 V (Supplementary Figs. 16 and 17). Likewise, the same experiment conducted under neutral pH conditions returns a predicted OCP of 0.03 V and a measured value of 0.03 V (Supplementary Fig. 19). The close agreement between the measured OCP values and those predicted from the independent electrochemical data on each half-reaction supports a mechanistic picture for nitrate hydrogenation that involves the electrochemical coupling of independent HOR and NO_3RR half-reactions.

Although these OCP data are highly suggestive of an electrochemical mechanism being operative during nitrate hydrogenation catalysis, they do not exclude an electrochemical mechanism proceeding in parallel with a classical thermochemical sequence for nitrate conversion. In this context, an electrochemical mechanism involves electron transfer between the catalyst and each substrate (H_2 and NO_3^-), while a thermochemical mechanism involves bimolecular recombination of surface-bound NO_3^* and surface H species. While the foregoing OCP measurements confirm that HOR and NO_3RR are operative during hydrogenation, a concurrent thermochemical mechanism would be invisible to this probe. To quantify the contribution of the electrochemical mechanism to the overall hydrogenation rate, we compared the rate of nitrate conversion predicted by the polarization data with the observed rate measured during hydrogenation catalysis.

Performing extended reaction measurements at the OCP, bulk conversion of nitrate to nitrite was achieved via reaction with H_2 using a PdCu/C catalyst immobilized on the same electrodes prepared for electrocatalytic measurements. Ultraviolet–visible (UV–vis) spectroscopy provides a convenient and reproducible route to quantifying mixed solutions of nitrate and nitrite (Fig. 2a); the method for peak identification and deconvolution of nitrate and nitrite peaks that allowed us to accurately quantify both species simultaneously is discussed in detail in Supplementary Methods and Supplementary Figs. 2–6. Using this method, nitrate consumption and nitrite generation are both measured during thermochemical catalysis at the PdCu/C GDE, with nitrite identified as the sole product under these conditions (Fig. 2b). This observation agrees with previous reports of the deactivation of subsequent nitrite hydrogenation under alkaline conditions for this alloy[44,45]. Based on this product distribution, we can now describe the two coupled half-reactions occurring at the OCP at

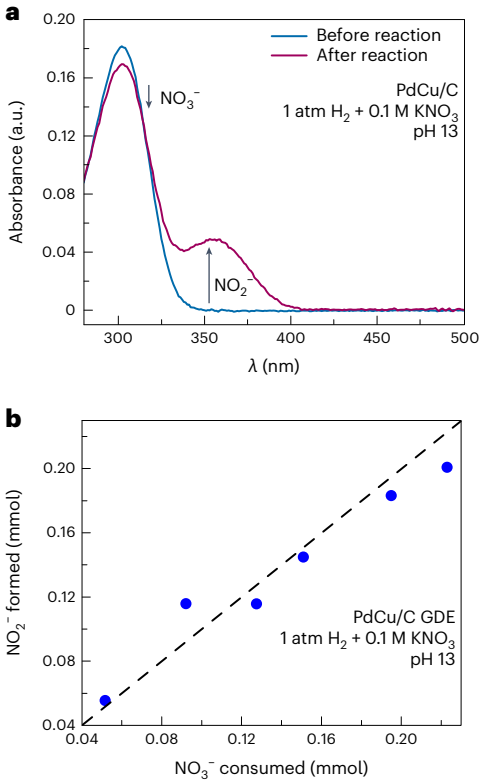

Fig. 2 | Nitrite is produced quantitatively in alkaline nitrate hydrogenation. **a**, Representative UV–vis spectra of a filtered reaction solution of 0.1 M KNO_3 in 0.2 M KOH. Spectra were collected before (blue) and after (purple) ~1 h of nitrate hydrogenation with PdCu/C. Nitrite is observed ca. 370 nm, and nitrate is observed ca. 300 nm. **b**, Measurements of nitrate consumption and nitrite formation at various timepoints during hydrogenation at PdCu/C GDE. Dashed line included as a visual aid to denote unity.

PdCu: the two-electron reduction of NO_3^- to NO_2^-, and the two-electron oxidation of H_2 to H^+.

$$NO_3^- + 2e^- + H_2O \rightarrow NO_2^- + 2OH^- \quad (1)$$

$$H_2 + 2OH^- \rightarrow 2e^- + 2H_2O \quad (2)$$

Armed with this electron stoichiometry, we can predict the thermal hydrogenation rate directly from the electrochemical polarization data, via the current passed by both half-reactions at the mixed potential (that is, the potential at which the current for the two half-reactions is exactly equal and opposite) (Fig. 1a). After running the hydrogenation, a thermal rate can be obtained via the disappearance of nitrate or the appearance of nitrite. Converting this rate to an effective current using the electron stoichiometry, the rate of nitrate conversion can be directly compared with the value predicted by the electrochemical data. If the major mechanism was invisible to our electrochemical probes and was thermochemical in nature, we would observe large differences in the measured and predicted reaction rates. On the other hand, if an electrochemical mechanism plays a substantial role in the total conversion, we would expect agreement between these rates. The polarization studies predict a current of 2.4 mA, which from the above electron stoichiometry equals 0.013 μmol s^{-1} of NO_3^-. A striking agreement is observed with the observed NO_3^- hydrogenation rate of 0.011 ± 0.001 μmol s^{-1}, which can be converted to an effective current of 2.1 ± 0.2 mA (Fig. 3). The same current-rate matching is reproduced at PdCu catalysts at 50:50 and 90:10 ratios of the two metals (Supplementary Fig. 18). These data indicate that nitrate hydrogenation at PdCu/C proceeds primarily via an electrochemical mechanism. Notably, our

https://doi.org/10.1038/s41929-023-01094-0

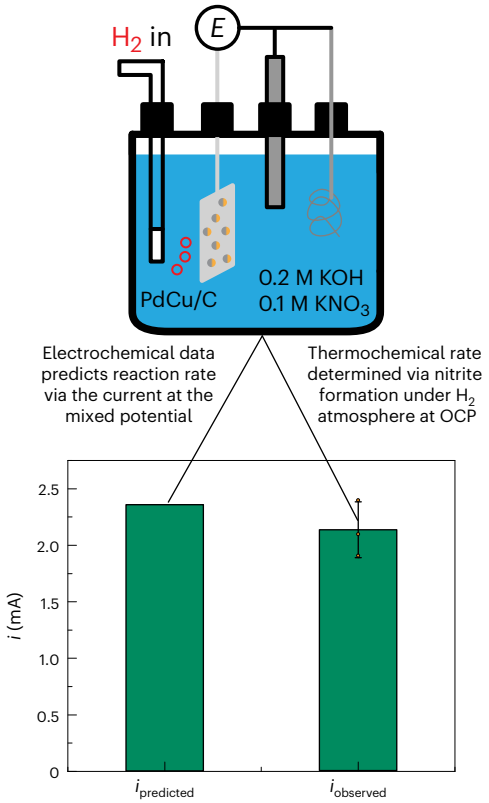

Fig. 3 | Electrochemical polarization data for PdCu/C predicts reaction rate. Comparison of predicted (left) and observed (right) reaction rates (reported in terms of current) for nitrate hydrogenation to nitrite at PdCu/C. Predicted reaction rate derived from electrochemical data described in Fig. 1. Observed reaction rate determined during hydrogenation at a PdCu/C GDE at open circuit in 0.2 M KOH + 0.1 M KNO_3 under 1 atm H_2. Error bar represents standard deviation of three replicate experiments, with the centre being the mean and dots representing rate measurements from each replicate experiment.

data do not differentiate a mechanism at Cu active sites involving a concerted proton-coupled electron transfer to adsorbed $NO_3^{\bullet}$, versus a mechanism first involving the formation of surface-H via H^+ and e^- at Cu that then recombines with bound NO_3^-. Both of these potential mechanisms would be viable in the context of a band-mediated mechanism, as both require the passage of electrons from Pd to Cu.

Pd and Cu execute orthogonal electrochemistry to hydrogenate NO_3^-

Critically, the data presented thus far on PdCu alloy catalysts do not contain any mechanistic information on the individual roles of Pd and Cu in the overall reaction. Initial insight into the role of each metal was obtained by comparing the OCP across a series of PdCu alloy catalysts of varying metal ratios. PdCu alloys were prepared using modified literature methods at different Pd/Cu ratios and dropcast onto carbon electrodes (see Supplementary Methods for details of characterization methods and Supplementary Figs. 7–15 for characterization of each PdCu alloy). First, polarization curves under both 1 atm H_2 and in 0.1 M KNO_3 were collected to generate a predicted OCP in the same manner as in Fig. 1 (Supplementary Fig. 16). Next, these alloy-decorated electrodes were exposed to thermochemical hydrogenation conditions while monitoring their potential at open circuit. Whereas the 10:90 alloy displays an OCP of 0.26 V, this value decreases to 0.17 V for the 50:50 alloy, and decreases further to 0.11 for the 90:10 alloy (Supplementary Fig. 17). This monotonic shift of 150 mV with increasing Pd content evinces a distinct electrochemical role for each of these metals. If both metals were competent for both half-reactions and displayed similar mixed potentials, we would expect no substantial shift in the overall potential of the alloy as a function of ratio of metal components. At the opposite extreme, if each metal was competent for only one half-reaction, then the OCP of the alloy should shift monotonically with alloy composition. A negative OCP shift indicates either that the oxidative half-reaction is accelerating or that the reductive half-reaction is decelerating, or both (see Supplementary Fig. 23 for a schematic diagram). We observe that the OCP shifts negatively as the Pd content increases, indicating that Pd is preferentially competent for the hydrogen oxidation half-reaction relative to Cu and vice versa.

Based on the preceding observation that each metal is not equally competent for each half-reaction, we investigated the most extreme case in which one alloy component is excluded entirely. As is well documented in the literature, almost all pure metals are completely inactive for nitrate hydrogenation[14,21]. However, based on the preceding data, we posited that each metal could be competent for one electrochemical half-reaction. Indeed, electrochemical polarization data of the two metals prepared as individual catalysts demonstrate the orthogonal reactivity of Pd and Cu. Pd/C and Cu/C electrodes were fabricated in the same manner as PdCu/C electrodes, and examined using the same electrochemical polarization protocol (Fig. 4). Under H_2, Pd displays onset of anodic catalytic current at 0 V versus RHE corresponding to HOR, rising to ca. 5 mA cm^{-2} at 0.1 V versus RHE (Fig. 4a, red). However, in nitrate solution, Pd displays minimal current enhancement relative to the Ar background (Fig. 4a, blue versus grey). The same experiments on Cu reveal the opposite reactivity profile, with catalytic current observed in nitrate solution at an onset potential of 0.3 V, rising to 20 mA cm^{-2} cathodic current at 0.1 V versus RHE (Fig. 4b, blue), but no catalytic current in the presence of H_2 alone (Fig. 4b, red versus

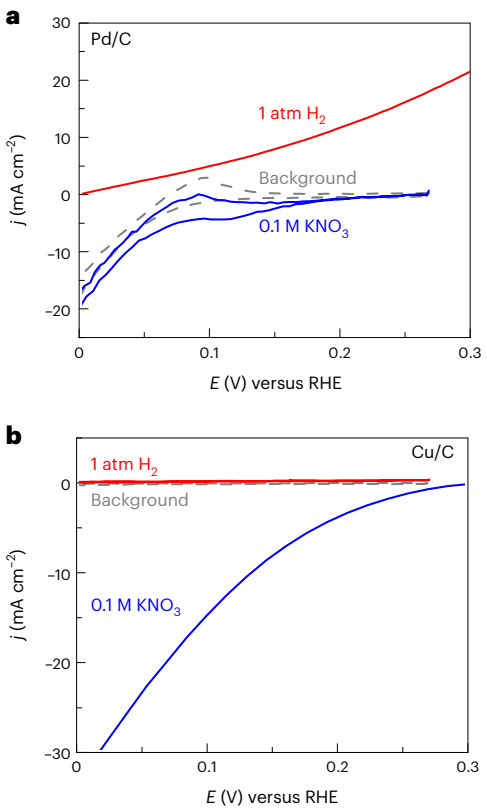

Fig. 4 | Polarization data for Pd/C and Cu/C reveals orthogonal electrochemical reactivity. a,**b**, Polarization curves for Pd/C (**a**) and Cu/C (**b**) electrodes recorded via LSV at 2 mv s^{-1} scan rate in 0.2 M KOH. Background traces (dashed grey) were collected under 1 atm Ar; 0.1 M KNO_3 traces (blue) were collected under 1 atm Ar; 1 atm H_2 traces (red) were collected in the absence of KNO_3.

https://doi.org/10.1038/s41929-023-01094-0

grey). These data, taken together with the studies above, suggest that in the PdCu alloy the role of Pd is to electrochemically oxidize H_2, and the role of Cu is to electrochemically reduce NO_3^-. It is still possible, as has been suggested previously, that bimetallic active sites also execute this reaction[16]. For example, reactive H atoms formed via H_2 dissociative adsorption at Pd may react with proximate NO_3^- activated at Cu to achieve the same transformation. However, these results strongly suggest that there is no necessity for these atomic-level interactions and that their presence confers no substantial catalytic promotion.

Based on this reaction orthogonality, we predict that nitrate hydrogenation can be catalysed by Pd and Cu at entirely separated interfaces, so long as an electronic conduction path is maintained between the two metals. Indeed, even for Pd/C and Cu/C catalysts that are macroscopically separated by an ion-exchange membrane, shorting the two catalysts is sufficient to drive net nitrate hydrogenation (Supplementary Fig. 20). Incorporating an ammeter, we observe current flow of ca. 0.5 mA during overall nitrate hydrogenation. By integrating the current flowing in this galvanic cell, we find that the charge passed matches the expected two-electron stoichiometry of nitrate reduction to nitrite (Supplementary Fig. 21). Taken together with our findings on PdCu/C, these results suggest that the predominant mechanism by which nitrate is hydrogenated to nitrite is via galvanic coupling between Pd-catalysed HOR and Cu-catalysed NO_3RR.

The foregoing data suggest a revision of the prevailing mechanistic picture of nitrate hydrogenation on PdCu bimetallic catalysts. Previously invoked ensemble effects such as spillover of H from Pd to Cu or bimetallic recombination of adsorbed H and surface-bound NO_3* at adjacent PdCu active sites are not necessary for nitrate hydrogenation. Instead, all that is necessary is an electrical pathway for current flow from Pd to Cu and ionic flow of proton equivalents in solution, rather than any atomic-level interaction between the two constituents. We stress that atomic-level interactions may confer a benefit in certain cases for nitrate hydrogenation catalysts; in particular, we are intrigued by the possibility that well-ordered intermetallic PdCu catalysts with greater proportions of bimetallic active sites may operate via a distinct mechanism. Nevertheless, on typical bimetallic catalysts with lesser degrees of order studied here and in the majority of literature reports, these results strongly support the notion that classical interpretations of bimetallic catalyst activity are insufficient to describe systems involving electrochemical coupling. In these systems, even spatially separated but electrically connected combinations of metals can execute reactivity inaccessible to either metal on its own.

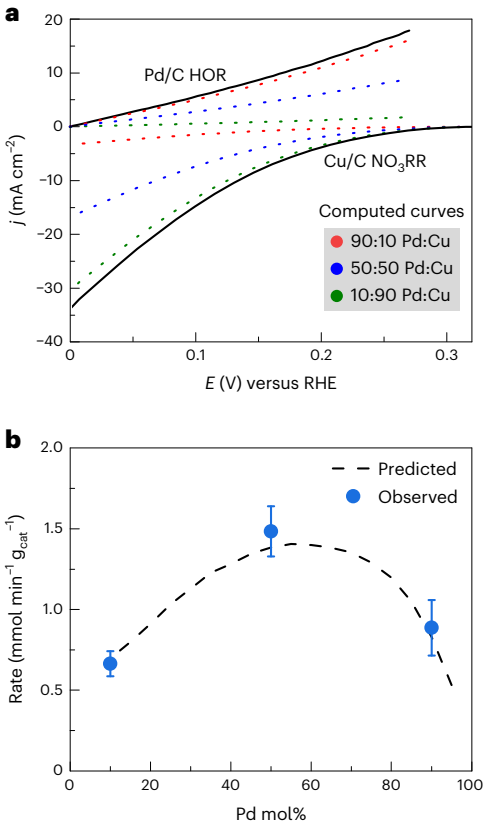

Fig. 5 | Pd/C and Cu/C polarization data directly predict PdCu/C hydrogenation rates. a, Decomposition of the Pd/C HOR trace and Cu/C NO_3RR trace as linear combinations; red dotted lines represent the simulated curve for a 90:10 Pd:Cu/C alloy, blue dotted lines represent the simulated curve for a 50:50 Pd:Cu/C alloy, and green dotted lines represent the simulated curve for a 10:90 Pd:Cu/C alloy (all ratios represent mol% of the metal constituent). Original LSV curves were taken at 2 mV s^{-1}. **b**, Comparison of predicted rates of nitrate hydrogenation at PdCu/C alloys between 10% and 95% Pd (black dashed curve), and observed rates at 10:90, 50:50 and 90:10 PdCu/C alloys (blue dots), measured in terms of millimoles nitrate consumed. Error bars represent standard deviation of three replicate experiments, with the centre points being the mean.

Individual metal electrochemistry predicts alloy activity

Based on our finding that half-reaction capabilities for nitrate hydrogenation at PdCu/C are segregated between the two metals, we next considered predicting the activity of any arbitrary alloy formulation just from the electrochemical behaviour of Pd/C and Cu/C. A recent study demonstrated that the polarization curves of various Au/Pt catalysts accurately predicts their thermocatalytic hydrogen peroxide synthesis activity[46]. We considered that this analysis may be advanced even further: for alloys that function via coupled half-reactions and in the absence of specific metal–metal interactions, the polarization curves of the pure metals alone should provide all of the requisite information for activity prediction, such that the collection of electrochemical data for every individual alloy ratio is not required. Using the electrochemical data for HOR on Pd/C and NO_3RR on Cu/C from Fig. 4, we simulated the polarization curves for PdCu/C alloys at a variety of different Pd:Cu molar ratios (from 10% to 95% Pd) with a constant total catalyst amount by linearly combining the individual metal polarization data. For example, to generate the simulated polarization curves for 50:50 PdCu, the Pd HOR and Cu NO_3RR polarization currents were multiplied by 0.5. Three of these simulated curves are depicted in Fig. 5a. This approach generated a series of calculated HOR and NO_3RR curves, to which we applied the potential and current matching condition to arrive at predicted rates of catalysis. Finally, we compared those rates to the observed rates for the 10:90, 50:50 and 90:10 PdCu alloys, notably maintaining experimental conditions as closely as possible to those used for measuring the polarization curves of the individual metals. We observed nitrate hydrogenation at a rate of 0.66 mmol min^{-1} g_{cat}^{-1} with 10:90 PdCu, 1.48 mmol min^{-1} g_{cat}^{-1} with 50:50 PdCu, and 0.89 mmol min^{-1} g_{cat}^{-1} with 90:10 PdCu. Gratifyingly, the observed rates match the predicted rates within experimental error (Fig. 5b), suggesting that the individual metal electrochemistry can accurately predict alloy thermochemical activity across a wide range of alloy ratios.

This analysis demonstrates that, not only is the activity of a given alloy accurately predicted by its own polarization behaviour, but that the polarization behaviour of the individual metals within the alloy also accurately predicts alloy activity. Prediction of hydrogenation rates from the electrochemical data on individual metals alone suggests that any alloying interactions between Pd and Cu have minimal impact on their respective abilities to catalyse HOR and NO_3RR, and thus have minimal impact on the overall hydrogenation activity. This finding has clear implications for alloy catalyst optimization; using just two electrochemical measurements, this analysis can predict a maximum in overall catalyst activity at ca. 50–60 mol% Pd content in the alloy. These data also demonstrate that a catalyst dilute in Cu has very similar nitrate hydrogenation activity to a catalyst dilute in

https://doi.org/10.1038/s41929-023-01094-0

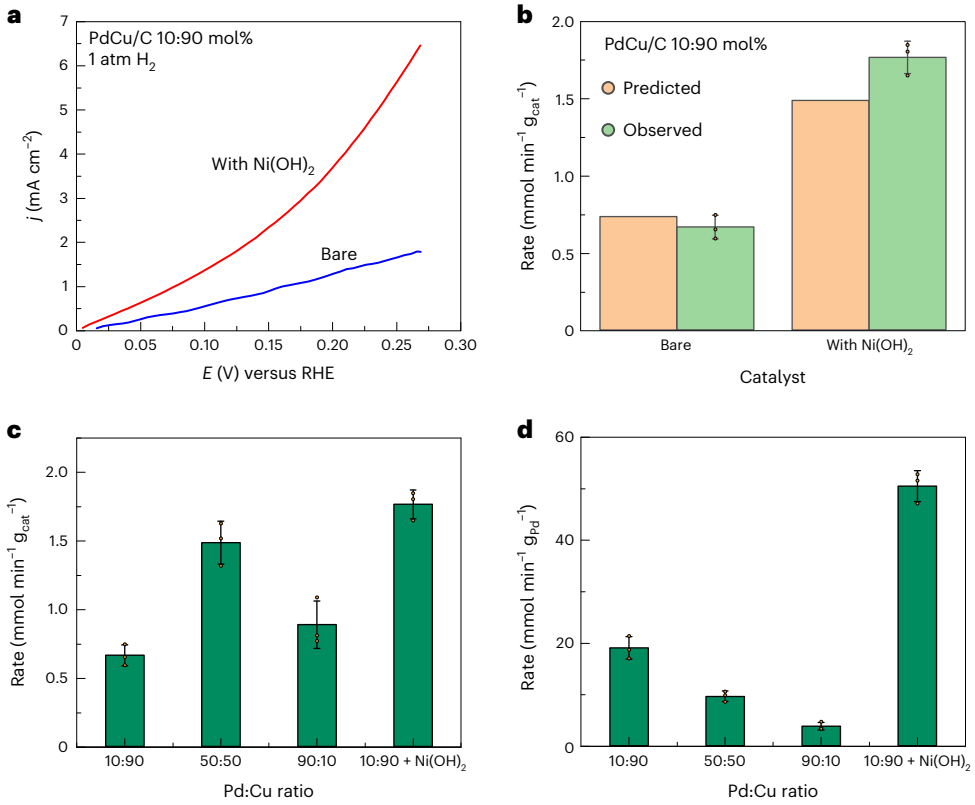

Fig. 6 | Targeted improvement of HOR via $Ni(OH)_2$ addition improves hydrogenation rate. a, Polarization curves for HOR for unmodified (blue) and $Ni(OH)_2$-modified (red) PdCu/C (10:90 mol% Pd:Cu). LSV curves were recorded at 2 mV s^{-1}. **b**, Predicted (from polarization data) (orange) and observed (green) nitrate hydrogenation rates at PdCu/C and $PdNi(OH)_2Cu/C$, measured in terms of millimoles nitrate consumed. **c**,**d**, Observed rates compared for different Pd:Cu formulations and $PdNi(OH)_2Cu/C$ on the basis of either g_{cat} (**c**) or g_{Pd} (**d**). Error bar represents standard deviation of three replicate experiments, with the centre being the mean and dots representing rate measurements from each replicate experiment.

Pd. Considering the ~5,000-fold difference in cost between the two metals[47], this analysis demonstrates an approach to predicting the optimal cost–performance ratio for these alloys, where an excess of Pd or another platinum group metal may not be required to still achieve reasonable catalytic rates.

The galvanic coupling model can be applied to understand reactivity trends across other materials as well. For example, when supported on insulating alumina, PtAg has been shown to display comparable activity to PdCu (ref. 19). This observation is at odds with the known superior activity of Pt over Pd for HOR[48] and comparable activity of Ag over Cu for NO_3RR catalysis[37], implying that the insulating support is impeding efficient galvanic coupling between Pt and Ag. We synthesized and measured the activity of PtAg/C at 50:50 mol% of Pt:Ag (Supplementary Fig. 24) and find an ~2-fold rate enhancement relative to PdCu/C, which is quantitatively predicted by the individual electrochemical profiles of Pt/C and Ag (Supplementary Fig. 22). Both PtAg/C and PdCu/C catalysts quantitatively produce nitrite in alkaline nitrate hydrogenation, with no reaction observed for nitrite hydrogenation (Supplementary Tables 3 and 4). Additionally, our electrochemical studies also revealed that Ru/C is competent for both HOR and NO_3RR, and consequently, we find that Ru/C has activity for nitrate hydrogenation, without the addition of a complementary metal (Supplementary Fig. 24). These findings suggest that galvanic coupling mechanisms may dominate for nitrate hydrogenation catalysis across diverse materials and highlight the power of electrochemical studies for understanding and predicting reactivity trends.

Galvanic coupling mechanism guides catalyst discovery

The galvanic coupling model implies that nitrate hydrogenation can be enhanced by promoting either of the underlying electrochemical half-reactions. Whereas catalyst additives such as amines and p-block elements have been explored previously for improving the activity of Pd- and Cu-containing catalysts for nitrate hydrogenation and other catalytic reactions[49–51], the connection we find in this work between electrochemical and thermochemical activity invites the use of catalyst additives not typically employed in thermal catalysis, but that have a potent effect in electrochemical catalysis. $Ni(OH)_2$ addition has been found to substantially improve exchange current densities for hydrogen evolution and hydrogen oxidation on Pt and Pd, with reported improvements as high as six- to eightfold[52–57]. Thus, we hypothesized that the addition of $Ni(OH)_2$ would improve the HOR activity of PdCu/C, leading to two predicted effects on thermal nitrate hydrogenation catalysis: a higher rate, and a more negative open-circuit potential. First, we compared the HOR activity of a PdCu (10:90) catalyst with the same catalyst modified with $Ni(OH)_2$ via a previously reported electrochemical formation procedure (Methods)[57]. We observe an improvement in catalyst activity of roughly threefold across the potential range measured (ca. 0–0.27 V versus RHE) (Fig. 6a). The NO_3RR activity, on the other hand, shows little change with the addition of $Ni(OH)_2$ (Supplementary Fig. 25). From the polarization curves, we predict a hydrogenation rate of 1.48 mmol min^{-1} g_{cat}^{-1} in the same manner as in Fig. 3 (Fig. 6b, orange bars). Next, we measured the thermal hydrogenation rate on this modified catalyst, while simultaneously monitoring catalyst potential in situ. We observe a shift in catalyst potential from unmodified to $Ni(OH)_2$-modified PdCu/C from 0.26 V to 0.18 V, and an improvement in rate from 0.66 mmol min^{-1} g_{cat}^{-1} to 1.76 mmol min^{-1} g_{cat}^{-1} (Fig. 6b). This modification produces a catalyst similar in activity to the best Pd:Cu ratio tested in this study, while using five times less palladium in the catalyst formulation (Fig. 6c,d). On a per-Pd basis, this catalyst has up to 13-fold improved activity relative to the other PdCu/C alloys

tested in this study, highlighting its value in maximizing the cost–performance ratio of PdCu. Our use of this additive is directly informed by the electrochemical nature of the nitrate hydrogenation mechanism; moreover, the catalyst modification specifically modulates the HOR activity of the catalyst, and the effect on thermochemical rate can be directly predicted from the electrochemical polarization behaviour. This strategy demonstrates the importance of considering both constituent half-reactions that make up an overall redox transformation, and how selective improvements to one half-reaction can produce a superior catalyst.

The foregoing studies establish a blueprint for alloy catalyst design that consists of breaking down a net thermochemical reaction into its constituent electrochemical half-reactions, identifying viable catalysts for each half-reaction, and combining these catalysts with an electrically conducting support either as isolated monometallic particles or multi-metallic particles to form alloy catalysts for the overall reaction. This strategy for discovering thermochemical bimetallic hydrogenation catalysts is generalizable, and is limited only by the scope of the electrochemical activity of the metals in the periodic table. As opposed to classical trial-and-error approaches for screening the large matrix of metal alloy combinations and composition ratios for net thermochemical activity, electrochemical analysis of the far smaller matrix of pure metals for each putative half-reaction provides the necessary information for identifying active alloy catalysts for the overall reaction. Indeed, in this case, the extensive existing electrochemical literature on nitrate reduction and hydrogen oxidation reactions was sufficient to identify high-activity materials for nitrate hydrogenation. We note that thermochemical nitrate hydrogenation has now been studied for three decades, with PdCu arguably remaining the state-of-the-art catalyst for that entire time[14,17,58,59]. Our electrochemical approach rapidly identified a catalyst material, PdNi(OH_2)Cu, that to the best of our knowledge has not been previously reported for this reaction. This approach may prove even more powerful when applied in oxidative thermal catalysis, where a wider array of metals (including non-noble metals) are active for the oxygen reduction half-reaction. This study highlights how electrochemical insights can be used to accelerate the discovery of thermochemical redox catalysts.

Conclusions

In this study, we employ an electrochemical toolkit to examine the mechanism of thermochemical nitrate hydrogenation, and create a framework for designing improved catalysts competent for this reaction. Specifically, electrochemical studies suggest that PdCu/C carries out nitrate hydrogenation via galvanic coupling of HOR occurring exclusively on Pd and NO_3RR occurring exclusively on Cu. These studies enable direct prediction of activity as a function of Pd:Cu ratio using only the polarization curves for bare Pd/C and Cu/C. These findings challenge the notion that intimate atomic-level contact between metals is critical to alloy reactivity and suggest that galvanic coupling may be a dominant mechanistic contributor. Employing these insights and leveraging known electrochemical reactivity trends, we rationally designed a material, PdNi($OH)_2$Cu/C, with enhanced activity at and reduced Pd loading relative to the state-of-the-art PdCu/C. Historically, the search for new bimetallic catalysts for a given reaction involves the exploration of a vast design space of potential choices in metal constituents, metal–metal ratio and support[60]. Classical approaches to design within these constraints consist of selecting the primary and dopant metals, followed by high-throughput screening to optimize parameters[60,61]. Because this catalyst test space can easily exceed hundreds or thousands of possible combinations, computational methods such as response surface methodology and machine learning are often employed to pare down to the most likely candidate catalysts[62–64]. Within this context, our work provides a complementary workflow for alloy catalyst design: breaking down thermal reactions into electrochemical half-reactions, identifying catalyst components with orthogonal, complementary electrochemical activity, and pairing these catalyst components to form an active multi-component catalyst. Thus, our findings advance electrochemical mechanisms for the catalytic reactivity of alloys that enable strategies for catalyst design and optimization for thermochemical redox transformations.

Methods

Chemicals and materials

The following chemicals were used as received; any chemicals or materials requiring additional preparation are described in their own subsection below. MilliQ water (Millipore Type 1, 18.2 MΩ cm) was used as the source of ultrapure water for all applications described below; potassium nitrate (KNO_3, Millipore Sigma, 99.999%); potassium nitrite (KNO_2, Millipore Sigma, >96.0%); potassium hydroxide (KOH, Millipore Sigma, 99.99%); potassium phosphate monobasic (KH_2PO_4, Millipore Sigma, 99.99%); potassium phosphate dibasic (K_2HPO_4, Millipore Sigma, 99.95%); titanium wire (Alfa Aesar, 0.25 mm, 99.7%); platinum mesh (VWR, 99.98%); platinum wire (VWR, 99.99%); silver foil (VWR, 99.9%); Nafion 117 (Ion Power, 178 µm); Nafion dispersion (Ion Power, 5 wt%); palladium chloride ($PdCl_2$, Millipore Sigma, 99.9%); silver nitrate ($AgNO_3$, Millipore Sigma, 99.9999%); ruthenium chloride ($RuCl_3$, Millipore Sigma, 99.98%); copper chloride dihydrate ($CuCl_2$, Millipore Sigma, 99.999%); activated carbon black (Vulcan XC-72R, Millipore Sigma); sodium hypophosphite ($NaPH_2O_2$, Millipore Sigma, 98%); sodium borohydride ($NaBH_4$, Millipore Sigma, 98%). Pre-fabricated Pt/C (60 wt%, 0.5 mg cm^{-2}), Pd/C (60 wt%, 0.5 mg cm^{-2}) and Cu/C (40 wt%, 0.2 mg cm^{-2}) GDEs and Pt/C (60 wt%) Pd/C (60 wt%) and Cu/C (40 wt%) powders were obtained from the Fuel Cell Store.

Preparation of Ag/AgCl reference electrode

A leakless Ag/AgCl reference electrode (EDAQ) was utilized in all experiments. Before experiments, the reference electrode was measured versus a pristine Ag/AgCl reference electrode to ensure a stable potential was maintained. In all cases, the leakless reference electrode was recorded to be within ~10 mV of the pristine Ag/AgCl reference. Before electrolysis, the electrode was rinsed with copious MilliQ water and dried under a stream of air. Following electrolysis, the electrode was rinsed with copious MilliQ water and stored in MilliQ water.

Preparation of Pt mesh counter electrode

A Pt mesh was threaded with Pt wire for use as a counter electrode. Before use, the counter electrode was flame annealed with a butane torch until glowing, then rinsed with copious MilliQ water.

Preparation of carbon-supported catalysts

Alloy catalyst powders used in this study (PdCu/C at various Pd:Cu ratios, PtAg/C) were prepared via a wet chemical reduction method similar to previously reported syntheses[3,36,65]. All catalysts were produced at a nominal total metal concentration of 25 wt% on activated carbon black. The full synthetic preparation method is provided below for 50:50 PdCu/C as a representative example. Other methods are described where they differ from this representative preparation.

Preparation of PdCu/C. Nominal molar ratios of 10:90, 50:50 and 90:10 Pd:Cu were used for each of the respective preparations. For the 50:50 PdCu catalyst preparation, $PdCl_2$ (51 mg of salt, 0.29 mmol of Pd, 31 mg of Pd) and $CuCl_2(H_2O)_2$ (51 mg of salt, 0.29 mmol of Cu, 19 mg of Cu) were dissolved in 20 ml MilliQ water. Total metal weight was 50 mg; 150 mg of activated carbon black and a stir bar were then added to the reaction vessel, followed by vigorous stirring and ultrasonication for 1 h to disperse the carbon substrate. An aqueous solution of the chemical reductant, sodium hypophosphite, was freshly prepared with at least tenfold excess relative to the total molar quantity of metal. In a representative preparation, 3 g of sodium hypophosphite (~34 mmol) was dissolved in 10 ml MilliQ water. This sodium hypophosphite solution

was then added dropwise to the stirring reaction vessel to reduce the metal precursor solutions. The reaction was stirred for 1 h and then filtered under vacuum. The black filtrate was washed with copious amounts of MilliQ water, dried under vacuum for 2 h and then further dried at 60 °C overnight in an oven. The filtered solution was clear, suggesting complete reduction of the metal precursors.

Preparation of PtAg/C. Instead of a simultaneous reduction, PtAg/C was prepared stepwise by first producing Pt/C and then reducing $AgNO_3$ onto the Pt/C substrate. This was done to avoid precipitation of AgCl during a simultaneous reduction. This procedure was used to prepare a carbon-supported catalyst with a 50:50 molar ratio of Pt:Ag.

Preparation of Cu/C. To obtain 50 mg of Cu on 150 mg of activated carbon black, 134 mg of the precursor copper chloride dihydrate was used. The synthesis proceeded in the same manner as that of PdCu/C, but sodium hypophosphite was found to be insufficiently reducing when only Cu was present, due to the observation of blue colouration in the filtrate. As a result, sodium borohydride was used, which presented a clear filtrate as expected.

Preparation of Pd/C. To obtain 50 mg of Pd on 150 mg of activated carbon black, 83 mg of the precursor palladium chloride was used. The synthesis then proceeded in the same manner as PdCu/C.

Preparation of Ru/C. To obtain 50 mg of Ru on 150 mg of activated carbon black, 102 mg of the precursor ruthenium chloride was used. The synthesis then proceeded in the same manner as Cu/C, using sodium borohydride as the reductant.

Electrode fabrication

For studies involving Pt/C, pre-fabricated GDEs were obtained from the Fuel Cell Store, similar to a previous study[31]. Pt/C was fabricated at 0.5 mg cm^{-2}, 60 wt%.These electrodes consisted of a sandwich of the catalyst layer, microporous carbon layer and gas diffusion layer. Each catalyst layer is composed of 60/40 wt% metal nanoparticles, 5–8 nm, supported on Vulcan XC-72. The microporous carbon layer is composed of a carbon black matrix, and the gas diffusion layer consisted of carbon cloth. These pre-fabricated catalysts/electrodes were used as received without further modification.

For studies involving alloy catalysts as well as Ru/C, Pd/C and Cu/C, electrodes were produced via dropcasting on a blank GDE substrate (Fuel Cell Store) to produce electrodes with varied nominal loadings of 1 mg cm^{-2}, 25 wt%. A prototypical preparation proceeded as follows to prepare a 1 mg cm^{-2} electrode: 5 mg of the desired catalyst on carbon was dispersed in a solution of 1 ml MilliQ water, 3.75 ml isopropanol and 0.25 ml Nafion dispersion in alcohol. One millilitre of this ink was dropcast in 100-µl droplet increments onto the blank GDE substrate over a hotplate set at 80 °C. The GDE was then dried overnight at 60 °C to remove residual solvent before use in electrochemical experiments.

For electrochemical experiments with an Ag foil, a 1-cm^2 foil (VWR, 99.99%) was first roughened according to a previous report[37]. Briefly, an alternating chronoamperometric pulse sequence was applied in 0.2 M KOH solution to the Ag foil, switching between 0 V and 0.4 V versus Ag/AgCl at a frequency of 50 Hz for 1.5 h. Then, a constant potential of −1.3 V was applied for 10 min.

To conduct the experiments producing Fig. 6 and Supplementary Fig. 25 with $PdNi(OH)_2Cu$, a PdCu/C electrode (10:90 mol%) was first prepared as described above at 1 mg cm^{-2} loading. Next, $Ni(OH)_2$ deposition was carried out using literature methods[53,55,57]. Briefly, the electrode was suspended in a 10 ml aqueous solution of 0.005 M $NiCl_2{\cdot}(H_2O)_6$ along with a Pt mesh counter electrode. Anodic polarization at constant current of 400 µA was conducted for 15 min, after which the electrode was rinsed with copious MilliQ water and re-introduced to 0.2 M KOH electrolyte for polarization and reaction testing.

Electrochemical methods

All electrochemical experiments, including LSV, cyclic voltammetry, OCP measurements and chronoamperometry were performed using a BioLogic potentiostat. For all LSVs provided in this work, a scan rate of 2 mV s^{-1} was used. Electrode potentials were converted to the reversible hydrogen electrode (E_{RHE}) scale using $E_{RHE} = E_{Ag/AgCl} + 0.20\ V + 0.06 \times pH$. Data are plotted versus RHE unless otherwise noted. Potentials were corrected for uncompensated Ohmic loss (iR_u) in situ via current interrupt at 90% of the measured value. R_u was measured using the current interrupt test function in the Biologic software. For the given cell configuration, R_u typically ranged from 5 to 10 Ω for all the electrolyte conditions. In a typical cell, this resulted in residual uncompensated resistance of ~1 Ω, which was ignored.

Electrochemical cell design and conditions

The reaction cell was composed of a hanging-strip (suspended from a current-collecting titanium wire, with the top edge of the GDE exposed to the headspace of the solution and otherwise submerged in solution) GDE working electrode (~1 cm^{-2}), a leakless Ag/AgCl reference electrode and a high surface area Pt-mesh counter electrode, similar to a previous study[4]. All experiments except for those generating Supplementary Fig. 21 were conducted in an custom-made electrochemical cell without separated counter compartment, equipped with reference electrode holder and a septum cap. The cell was cleaned with copious amounts of MilliQ water before each experiment. Either 0.2 M KOH or 0.5 M phosphate buffer (10.0 ml total volume) was employed as the supporting electrolyte. The desired gas (ultrahigh-purity Ar or H_2) was flowed into the working compartment of the reaction cell at a flow rate of 20 SCCM ($cm^3\ min^{-1}$), using a series of mass-flow controllers (Alicat Scientific) affixed to each gas line, with gas directly bubbling into solution for at least 10 min before any measurement, and then continuously bubbled during experiments, with gas transport facilitated by the small exposed section of the GDE. All experiments were performed at ambient temperature. All cells were equipped with a small stir bar, with vigorous stirring during polarization. For electrochemical experiments in which two compartments were desired, a custom-made electrochemical H-cell was used, equipped with a Nafion 117 membrane separator.

For the data in Supplementary Fig. 21, Pd/C and Cu/C electrodes were separated into different compartments of an H-cell equipped with a Nafion 117 membrane separator. Then, the electrodes were connected as follows: working electrode clip was connected to the Cu electrode, counter and reference clips were connected to the Pd electrode, and counter sense clip was connected to a leakless Ag/AgCl reference electrode. Then, H_2 was bubbled through the compartment containing Pd, while Ar was bubbled through the compartment containing the Cu electrode. For the single compartment cell, H_2 was bubbled through the entire cell. After gas equilibration, 0.5 M KNO_3 was introduced via a concentrated stock solution into the Cu electrode compartment. Then, the potentiostat was employed as an ammeter by setting a chronoamperometry experiment applying a potential of 0 V versus the reference (in this case, the reference and counter both being Pd). This applied potential was then referenced versus the leakless Ag/AgCl reference. Following the application of this potential, periodic aliquots were taken and analysed for nitrate consumption over time. Nitrate consumption was then compared against the charge passed through the circuit to determine electron stoichiometry.

Thermochemical experiments

Thermochemical experiments refer to catalyst testing in the absence of applied polarization. For the experiments producing the data in Figs. 3, 5 and 6, we conducted these experiments in experimental conditions that matched, as closely as possible, the conditions for electrochemical testing, such that transport conditions were maintained and such

that rates could be quantitatively compared between electrochemical and thermochemical tests. Thermochemical experiments were carried out in a two-electrode cell, as no polarization was applied in these experiments; only potential measurement was needed. Catalyst electrodes, prepared in the same way as for electrochemical testing, were suspended in a hanging-strip configuration. Next, H_2 was bubbled through the entire cell, consisting of 9 ml of 0.2 M KOH, for at least 10 min, while measuring the potential of the catalyst versus a leakless Ag/AgCl reference electrode. To initiate thermochemical nitrate hydrogenation, 1 ml of 1 M KNO_3 in 0.2 M KOH was introduced to the solution with a syringe. Two timepoints were taken to determine reaction progress via 1-ml aliquots taken at ca. 15 and 30 min of reaction. This same method was used to generate the data in Supplementary Fig. 24 (rate measurements for mono- and bimetallic catalysts as well as $Ni(OH)_2$-modified PdCu). All rate measurements were collected at low conversion (<10%) to limit substrate consumption.

Product analysis

To evaluate the selectivity of alloy catalysts towards ammonium and nitrite, higher conversions were required to be able to measure ammonium via nuclear magnetic resonance (NMR) quantification. For these experiments that produced the data in Supplementary Table 3, 5 mg of the desired catalyst was dispersed in 9 ml of 0.2 M KOH, stirred vigorously and sonicated to achieve a uniform dispersion, and then stirred continuously during reaction. To initiate thermochemical nitrate hydrogenation, H_2 gas was bubbled into solution at 20 SCCM, and then 10 mM nitrate was introduced as a 1-ml aliquot from a 100 mM stock solution of KNO_3 in 0.2 M KOH. Three timepoints were taken to determine reaction progress and product selectivity in 1-ml aliquots taken at ca. 15, 30 and 45 min of reaction. Ammonium selectivity was measured in this way because larger conversions were required to quantify this product via NMR; as a result, larger catalyst loadings were required than what could be achieved on electrodes, so dispersed catalysts were employed.

During both electrochemical and thermochemical experiments, periodic 1-ml aliquots were collected and filtered to determine reaction rate and detect product formation. In all experiments carried out in the primary electrolyte system (0.2 M KOH), nitrite (NO_2^-) was determined to be the quantitative product of reaction on all catalysts at all timepoints. This quantification was carried out using UV–vis spectroscopy. For more information, see 'UV–vis spectroscopy to quantify nitrate and nitrite' section.

Nitrate hydrogenation can produce a multitude of products including NO_2^-, NO, NO_2, N_2 and NH_3, but previous reports have similarly determined nitrite to be the quantitative or near-quantitative product when operating in alkaline media[9]. For all reactions in 0.2 M KOH, nitrite was found to match the total nitrate consumption to within 5% (for example, between 95% and 105% molar selectivity), obviating the need for additional product quantification. Nevertheless, NMR spectra of reaction solutions following nitrate hydrogenation to nitrite over PdCu/C and PtAg/C in 0.2 M KOH were collected following the methods described below and showed no formation of ammonia.

We quantified the ammonia present in reaction aliquots using the following procedure. First, the thermochemical reaction was conducted as described above with the addition of a solution of 1 M HCl at the outflow of the reaction vial to serve as an acid trap for any gaseous NH_3 formed. Next, 250 µl of the reaction solution was aliquoted following 15 min of reaction and the catalyst was filtered to terminate the reaction. To this aliquot, we added 250 µl of a solution of 1 M HCl with added 20 mM maleic acid. This procedure served two purposes: first, it ensured full protonation of any ammonia formed to enable detection of the ammonium ion via ^{1}H NMR, and second, the addition of maleic acid served as an internal NMR integration standard. Finally, 50 µl of d_6-dimethyl sulfoxide was added to provide a suitable locking solvent. Both the reaction vial and trap were aliquoted at all timepoints measured. Ammonium appears as a triplet ca. 7.2 ppm, and was integrated relative to the C–H resonance of the maleic acid internal standard. NMR experiments were collected with a delay time of 10 s to ensure quantitative signal recovery, and 64 scans. A representative spectrum of ammonium with the maleic acid internal standard is provided in Supplementary Fig. 1.

UV–vis spectroscopy to quantify NO_3^- and NO_2^-

To quantify the concentration of nitrate (NO_3^-) and nitrite (NO_2^-) in mixed solutions with electrolyte, UV–vis spectroscopy was employed using a Cary 60 UV–vis spectrometer and disposable 1 cm path length UV–vis cell. Both nitrate and nitrite display electronic absorption signatures in the UV–vis region with λ_{max} of 300 and 360 nm, respectively. At 0.1 M concentration, peak absorbance values for nitrate were ca. 0.7 absorbance units; for nitrite at 0.05 M concentration, peak absorbances were ca. 1.0 absorbance units. Through independent measurements, both species were found to obey linear Beer's Law behaviour for their peak absorbance as a function of concentration in this absorption range (Supplementary Figs. 4 and 5). As a result, reaction aliquots could be analysed undiluted, with typical absorbances for these two species within 0–1.0 absorbance units.

To accurately quantify both species, peak overlap was corrected for. At 0.1 M concentration, nitrate has 0 absorbance at the peak absorbance wavelength for nitrite; as such, the nitrite absorbance is not convoluted by even the maximum amount of nitrate (Supplementary Fig. 2). Nitrite, on the other hand, has a distinct shoulder in its UV–vis spectrum (Supplementary Fig. 3). This shoulder feature leads to a convolution in the nitrate absorbance, resulting in an overlap of the native nitrate absorbance with absorbance from nitrite. To correct for this difference, a third Beer's Law plot was constructed for the absorbance of nitrite at the λ_{max} of nitrate (Supplementary Fig. 6). This relation was used to subtract nitrite contribution from the absorbance for nitrate, resulting in simultaneous product quantification of nitrate and nitrite. To the best of our knowledge, this is the first use of this approach to quantify these products of nitrate hydrogenation. This approach is valid only above ca. 1 mM concentrations of nitrate, below which the absorbance is too low for accurate quantification. For our purposes, this corresponded to either 99% conversion (for electrochemical experiments at 0.1 M KNO_3) or 90% conversion (for thermochemical experiments at 0.01 M KNO_3); as a result, we employ this method throughout our analysis.

Using the Beer's Law plots in Supplementary Figs. 4–6, and Supplementary Equations 1 and 2 can be used to determine nitrate and nitrite concentrations in mixed solutions of the two species with a cuvette of 1 cm path length. To validate this quantification approach, mixed solutions of nitrate and nitrite at known concentrations were prepared, and their analytical concentrations were compared against calculated nitrate and nitrite concentrations using the measured absorbances in Supplementary Table 1. Based on the very close agreement in calculated and analytical concentrations, this method of quantification accurately determines nitrate and nitrite concentrations in solutions typical of those produced during catalytic experiments.

Additional supplementary information, including details of catalyst characterization can be found in Supplementary Methods.

Data availability

The data that support the findings of this study are included in the published article (and its Supplementary Information), with raw source data (cyclic voltammetry, potentiometry and rate measurements) available in an accompanying source data file, or available from the authors on reasonable request. Source data are provided with this paper.

References

1. Park, K.-W. et al. Chemical and electronic effects of Ni in Pt/Ni and Pt/Ru/Ni alloy nanoparticles in methanol electrooxidation. *J. Phys. Chem. B* **106**, 1869–1877 (2002).

2. Qin, L. et al. Cooperative catalytic performance of bimetallic Ni–Au nanocatalyst for highly efficient hydrogenation of nitroaromatics and corresponding mechanism insight. *Appl. Catal. B* **259**, 118035 (2019).
3. Muneeb, O. et al. Electrochemical oxidation of polyalcohols in alkaline media on palladium catalysts promoted by the addition of copper. *Electrochim. Acta* **218**, 133–139 (2016).
4. Wang, H. et al. Platinum-modulated cobalt nanocatalysts for low-temperature aqueous-phase Fischer–Tropsch synthesis. *J. Am. Chem. Soc.* **135**, 4149–4158 (2013).
5. Lortie, M., Isaifan, R., Liu, Y. & Mommers, S. Synthesis of CuNi/C and CuNi/γ-Al_2O_3 catalysts for the reverse water gas shift reaction. *Int. J. Chem. Eng.* **2015**, 1–9 (2015).
6. Li, H., Shin, K. & Henkelman, G. Effects of ensembles, ligand, and strain on adsorbate binding to alloy surfaces. *J. Chem. Phys.* **149**, 174705 (2018).
7. Li, H. et al. Oxygen reduction reaction on classically immiscible bimetallics: a case study of RhAu. *J. Phys. Chem. C* **122**, 2712–2716 (2018).
8. Takehiro, N., Liu, P., Bergbreiter, A., Nørskov, J. K. & Behm, R. J. Hydrogen adsorption on bimetallic PdAu(111) surface alloys: minimum adsorption ensemble, ligand and ensemble effects, and ensemble confinement. *Phys. Chem. Chem. Phys.* **16**, 23930–23943 (2014).
9. Mavrikakis, M., Hammer, B. & Nørskov, J. K. Effect of strain on the reactivity of metal surfaces. *Phys. Rev. Lett.* **81**, 2819–2822 (1998).
10. Zhang, L. & Henkelman, G. Tuning the oxygen reduction activity of Pd shell nanoparticles with random alloy cores. *J. Phys. Chem. C* **116**, 20860–20865 (2012).
11. García-Muelas, R. & López, N. Statistical learning goes beyond the d-band model providing the thermochemistry of adsorbates on transition metals. *Nat. Commun.* **10**, 4687 (2019).
12. Yao, Y. & Goodman, D. W. Direct evidence of hydrogen spillover from Ni to Cu on Ni–Cu bimetallic catalysts. *J. Mol. Catal. Chem.* **383–384**, 239–242 (2014).
13. Fischer, A. F. & Iglesia, E. The nature of "hydrogen spillover": site proximity effects and gaseous intermediates in hydrogenation reactions mediated by inhibitor-scavenging mechanisms. *J. Catal.* **420**, 68–88 (2023).
14. Hörold, S., Tacke, T. & Vorlop, K. Catalytical removal of nitrate and nitrite from drinking water: 1. Screening for hydrogenation catalysts and influence of reaction conditions on activity and selectivity. *J. Environ. Technol.* **14**, 931–939 (1993).
15. Wang, Z., Richards, D. & Singh, N. Recent discoveries in the reaction mechanism of heterogeneous electrocatalytic nitrate reduction. *Catal. Sci. Technol.* **11**, 705–725 (2021).
16. Pintar, A., Batista, J., Levec, J. & Kajiuchi, T. Kinetics of the catalytic liquid-phase hydrogenation of aqueous nitrate solutions. *Appl. Catal. B* **11**, 81–98 (1996).
17. Martínez, J., Ortiz, A. & Ortiz, I. State-of-the-art and perspectives of the catalytic and electrocatalytic reduction of aqueous nitrates. *Appl. Catal. B* **207**, 42–59 (2017).
18. Xie, Y., Cao, H., Li, Y., Zhang, Y. & Crittenden, J. C. Highly selective PdCu/amorphous silica–alumina (ASA) catalysts for groundwater denitration. *Environ. Sci. Technol.* **45**, 4066–4072 (2011).
19. Gauthard, F., Epron, F. & Barbier, J. Palladium and platinum-based catalysts in the catalytic reduction of nitrate in water: effect of copper, silver, or gold addition. *J. Catal.* **220**, 182–191 (2003).
20. Pintar, A., Batista, J. & Muševič, I. Palladium-copper and palladium-tin catalysts in the liquid phase nitrate hydrogenation in a batch-recycle reactor. *Appl. Catal. B* **52**, 49–60 (2004).
21. Prüsse, U. & Vorlop, K. D. Supported bimetallic palladium catalysts for water-phase nitrate reduction. *J. Mol. Catal. Chem.* **173**, 313–328 (2001).
22. Sá, J. & Vinek, H. Catalytic hydrogenation of nitrates in water over a bimetallic catalyst. *Appl. Catal. B* **57**, 247–256 (2005).
23. Cai, F. et al. Preparation of PdCu alloy nanocatalysts for nitrate hydrogenation and carbon monoxide oxidation. *Catalysts* **6**, 96 (2016).
24. Wang, Z., Ortiz, E. M., Goldsmith, B. R. & Singh, N. Comparing electrocatalytic and thermocatalytic conversion of nitrate on platinum–ruthenium alloys. *Catal. Sci. Technol.* **11**, 7098–7109 (2021).
25. Ilinich, O. M., Gribov, E. N. & Simonov, P. A. Water denitrification over catalytic membranes: hydrogen spillover and catalytic activity of macroporous membranes loaded with Pd and Cu. *Catal. Today* **82**, 49–56 (2003).
26. Yoshinaga, Y., Akita, T., Mikami, I. & Okuhara, T. Hydrogenation of nitrate in water to nitrogen over Pd–Cu supported on active carbon. *J. Catal.* **207**, 37–45 (2002).
27. Keresszegi, C., Bürgi, T., Mallat, T. & Baiker, A. On the role of oxygen in the liquid-phase aerobic oxidation of alcohols on palladium. *J. Catal.* **211**, 244–251 (2002).
28. Mallat, T. & Baiker, A. Catalyst potential measurement: a valuable tool for understanding and controlling liquid phase redox reactions. *Top. Catal.* **8**, 115–124 (1999).
29. An, H., Sun, G., Hülsey, M. J., Sautet, P. & Yan, N. Demonstrating the electron–proton-transfer mechanism of aqueous phase 4-nitrophenol hydrogenation using unbiased electrochemical cells. *ACS Catal.* **12**, 15021–15027 (2022).
30. Fortunato, G. V. et al. Analysing the relationship between the fields of thermo- and electrocatalysis taking hydrogen peroxide as a case study. *Nat. Commun.* **13**, 1973 (2022).
31. Ryu, J. et al. Thermochemical aerobic oxidation catalysis in water can be analysed as two coupled electrochemical half-reactions. *Nat. Catal.* **4**, 742–752 (2021).
32. Adams, J. S., Kromer, M. L., Rodríguez-López, J. & Flaherty, D. W. Unifying concepts in electro- and thermocatalysis toward hydrogen peroxide production. *J. Am. Chem. Soc.* **143**, 7940–7957 (2021).
33. Yamanaka, I., Onizawa, T., Takenaka, S. & Otsuka, K. Direct and continuous production of hydrogen peroxide with 93% selectivity using a fuel-cell system. *Angew. Chem. Int. Ed.* **42**, 3653–3655 (2003).
34. Howland, W. C., Gerken, J. B., Stahl, S. S. & Surendranath, Y. Thermal hydroquinone oxidation on Co/N-doped carbon proceeds by a band-mediated electrochemical mechanism. *J. Am. Chem. Soc.* **144**, 11253–11262 (2022).
35. Zhao, X. et al. Chemo-bio catalysis using carbon supports: application in H_2-driven cofactor recycling. *Chem. Sci.* **12**, 8105–8114 (2021).
36. Huang, X. et al. Au–Pd separation enhances bimetallic catalysis of alcohol oxidation. *Nature* **603**, 271–275 (2022).
37. Liu, H. et al. Electrocatalytic nitrate reduction on oxide-derived silver with tunable selectivity to nitrite and ammonia. *ACS Catal.* **11**, 8431–8442 (2021).
38. Liu, M. J. et al. Catalytic performance and near-surface X-ray characterization of titanium hydride electrodes for the electrochemical nitrate reduction reaction. *J. Am. Chem. Soc.* **144**, 5739–5744 (2022).
39. Teng, W. et al. Selective nitrate reduction to dinitrogen by electrocatalysis on nanoscale iron encapsulated in mesoporous carbon. *Environ. Sci. Technol.* **52**, 230–236 (2018).
40. Li, J. et al. Efficient ammonia electrosynthesis from nitrate on strained ruthenium nanoclusters. *J. Am. Chem. Soc.* **142**, 7036–7046 (2020).
41. Butcher, D. P. & Gewirth, A. A. Nitrate reduction pathways on Cu single crystal surfaces: effect of oxide and Cl^-. *Nano Energy* **29**, 457–465 (2016).

42. Power, G. P., Staunton, W. P. & Ritchie, I. M. Mixed potential measurements in the elucidation of corrosion mechanisms—II. Some measurements. *Electrochim. Acta* **27**, 165–169 (1982).
43. Wagner, C. & Traud, W. Über die Deutung von Korrosionsvorgängen durch Überlagerung von elektrochemischen Teilvorgängen und über die Potentialbildung an Mischelektroden. *Z. Elektrochem. Angew. Phys. Chem.* **44**, 391–402 (1938).
44. Vorlop, K.-D. & Prüsse, U. in *Environmental Catalysis* Vol. 1 (eds Janssen, F. J. J. G. & van Santen, R. A.) 195–218 (Imperial College Press, 1999).
45. Pintar, A. & Batista, J. Catalytic stepwise nitrate hydrogenation in batch-recycle fixed-bed reactors. *J. Hazard. Mater.* **149**, 387–398 (2007).
46. Zhao, Y. et al. Electrochemical screening of Au/Pt catalysts for the thermocatalytic synthesis of hydrogen peroxide based on their oxygen reduction and hydrogen oxidation activities probed via voltammetric scanning electrochemical microscopy. *ACS Sustain. Chem. Eng.* **10**, 17207–17220 (2022).
47. Precious and industrial metals. *Bloomberg* https://www.bloomberg.com/markets/commodities/futures/metals (2023).
48. Ohyama, J., Kumada, D. & Satsuma, A. Improved hydrogen oxidation reaction under alkaline conditions by ruthenium–iridium alloyed nanoparticles. *J. Mater. Chem. A* **4**, 15980–15985 (2016).
49. Sun, W. et al. Elevated N_2 selectivity in catalytic denitrification by amino group-assisted in-situ buffering effect of NH_2–SiO_2 supported PdCu bimetallic nanocatalyst. *Chem. Eng. J.* **390**, 124617 (2020).
50. Wang, K.-W. et al. Promotion of PdCu/C catalysts for ethanol oxidation in alkaline solution by SnO_2 modifier. *ChemCatChem* **4**, 1154–1161 (2012).
51. Bansode, A., Tidona, B., Rohr, P. Rvon & Urakawa, A. Impact of K and Ba promoters on CO_2 hydrogenation over Cu/Al_2O_3 catalysts at high pressure. *Catal. Sci. Technol.* **3**, 767–778 (2013).
52. Subbaraman, R. et al. Trends in activity for the water electrolyser reactions on 3d M(Ni,Co,Fe,Mn) hydr(oxy)oxide catalysts. *Nat. Mater.* **11**, 550–557 (2012).
53. Subbaraman, R. et al. Enhancing hydrogen evolution activity in water splitting by tailoring Li^+–$Ni(OH)_2$–Pt Interfaces. *Science* **334**, 1256–1260 (2011).
54. Danilovic, N. et al. Enhancing the alkaline hydrogen evolution reaction activity through the bifunctionality of $Ni(OH)_2$/metal catalysts. *Angew. Chem. Int. Ed.* **51**, 12495–12498 (2012).
55. Ledezma-Yanez, I. et al. Interfacial water reorganization as a pH-dependent descriptor of the hydrogen evolution rate on platinum electrodes. *Nat. Energy* **2**, 17031 (2017).
56. McCrum, I. T. & Koper, M. T. M. The role of adsorbed hydroxide in hydrogen evolution reaction kinetics on modified platinum. *Nat. Energy* **5**, 891–899 (2020).
57. Tang, B. Y., Bisbey, R. P., Lodaya, K. M., Toh, W. L. & Surendranath, Y. Reaction environment impacts charge transfer but not chemical reaction steps in hydrogen evolution catalysis. *Nat. Catal.* **6**, 339–350 (2023).
58. Zhao, F., Xin, J., Yuan, M., Wang, L. & Wang, X. A critical review of existing mechanisms and strategies to enhance N_2 selectivity in groundwater nitrate reduction. *Water Res.* **209**, 117889 (2022).
59. Tokazhanov, G., Ramazanova, E., Hamid, S., Bae, S. & Lee, W. Advances in the catalytic reduction of nitrate by metallic catalysts for high efficiency and N_2 selectivity: a review. *Chem. Eng. J.* **384**, 123252 (2020).
60. Ras, E.-J. & Rothenberg, G. Heterogeneous catalyst discovery using 21st century tools: a tutorial. *RSC Adv.* **4**, 5963–5974 (2014).
61. Fan, J. et al. Recent progress on rational design of bimetallic Pd based catalysts and their advanced catalysis. *ACS Catal.* **10**, 13560–13583 (2020).
62. Li, Z., Wang, S., Chin, W. S., Achenie, L. E. & Xin, H. High-throughput screening of bimetallic catalysts enabled by machine learning. *J. Mater. Chem. A* **5**, 24131–24138 (2017).
63. Sun, Y., Wei, J., Zhang, J. P. & Yang, G. Optimization using response surface methodology and kinetic study of Fischer–Tropsch synthesis using SiO_2 supported bimetallic Co–Ni catalyst. *J. Nat. Gas. Sci. Eng.* **28**, 173–183 (2016).
64. Udumula, V. et al. Dual optimization approach to bimetallic nanoparticle catalysis: impact of M1/M2 ratio and supporting polymer structure on reactivity. *ACS Catal.* **5**, 3457–3462 (2015).
65. Muneeb, O., Do, E., Boyd, D., Perez, J. & Haan, J. L. PdCu/C anode catalysts for the alkaline ascorbate fuel cell. *Appl. Energy* **235**, 473–479 (2019).

Acknowledgements

We thank T. Wesley, W. Howland, M. Huelsey, A. Chu, A. Borisov, H.-X. Wang, D. Harraz, N. Razdan, R. Zeng and the Surendranath Lab for helpful discussions and manuscript feedback. This work was primarily supported by the Air Force Office of Scientific Research (AFOSR) under award number FA9550-20-1-0291. K.M.L., S.W. and K.S.W. acknowledge support from the National Science Foundation Graduate Fellowship.

Author contributions

K.M.L., B.Y.T., R.P.B., J.R. and Y.S. conceived the research and developed experiments. K.M.L. and B.Y.T. conducted all electrochemical and thermochemical experiments. K.M.L., B.Y.T., S.W. and K.S.W. conducted catalyst characterization measurements. W.L.T. 3D printed prototype cell designs for experiments. K.M.L., B.Y.T. and Y.S. wrote the manuscript with input from all authors. Y.R.-L. and Y.S. provided laboratory space and instrumentation.

Competing interests

The authors declare no competing interests.

Additional information

Supplementary information The online version contains supplementary material available at https://doi.org/10.1038/s41929-023-01094-0.

Correspondence and requests for materials should be addressed to Yogesh Surendranath.

Peer review information *Nature Catalysis* thanks Bin Zhang and the other, anonymous, reviewer(s) for their contribution to the peer review of this work.